THE JOURNAL OF BIOLOGICAL CHEMISTRY VOL. 282, NO. 8, pp. 5749–5760, February 23, 2007

Mutation Analysis of the Short Cytoplasmic Domain of the Cell-Cell Adhesion Molecule CEACAM1 Identifies Residues That Orchestrate Actin Binding and Lumen Formation*[S]

Received for publication, November 27, 2006, and in revised form, December 21, 2006 Published, JBC Papers in Press, December 27, 2006, DOI 10.1074/jbc.M610903200

Charng-Jui Chen[‡1], **Julia Kirshner**[‡1,2], **Mark A. Sherman**[§], **Weidong Hu**[‡], **Tung Nguyen**[‡], **and John E. Shively**[‡3]

From the Divisions of [‡]*Immunology and* [§]*Information Sciences, Beckman Research Institute of the City of Hope, Duarte, California 91010*

CEACAM1–4S (carcinoembryonic antigen cell adhesion molecule 1, with 4 ectodomains and a short, 12–14 amino acid cytoplasmic domain) mediates lumen formation via an apoptotic and cytoskeletal reorganization mechanism when mammary epithelial cells are grown in a three-dimensional model of mammary morphogenesis. We show by quantitative yeast two-hybrid, BIAcore, NMR HSQC and STD, and confocal analyses that amino acids phenylalanine (Phe^{454}) and lysine (Lys^{456}) are key residues that interact with actin orchestrating the cytoskeletal reorganization. A CEACAM1 membrane model based on vitamin D-binding protein that predicts an interaction of Phe^{454} at subdomain 3 of actin was supported by inhibition of binding of actin to vitamin D-binding protein by the cytoplasmic domain peptide. We also show that residues Thr^{457} and/or Ser^{459} are phosphorylated in CEACAM1-transfected cells grown in three-dimensional culture and that mutation analysis of these residues (T457A/S459A) or F454A blocks lumen formation. These studies demonstrate that a short cytoplasmic domain membrane receptor can directly mediate substantial intracellular signaling.

CEACAM1[4] (carcinoembryonic antigen cell adhesion molecule 1) is a type I membrane glycoprotein that mediates homotypic cell adhesion and belongs to the *CEA* gene family (1). It has been shown to play a role in bacterial and viral uptake (2–5), in insulin clearance (6), angiogenesis (7), NK and T-cell regulation (8–11), and tumor suppression (12, 13). Despite its proposed function as a cell-cell adhesion molecule, CEACAM1 is often found on the lumenal surface of epithelial cells, suggesting the possibility that it also plays a role in cell polarization and lumen formation. In this respect, we have recently shown that CEACAM1 is expressed on the lumenal surface of normal mammary epithelial cells (14), and that in a three-dimensional model of mammary morphogenesis, blocking its expression with either an antisense gene or anti-CEACAM1 antibodies blocks lumen formation (15, 16), while breast cancer cells, which lack CEACAM1 and fail to form lumena in a three-dimensional culture, are restored to normal when transfected with the epithelial specific CEACAM1–4S isoform (16). *CEACAM1* gene expression has been shown to be down-regulated early in colon cancer (12, 17), and in a variety of cancer models, re-introduction of the *CEACAM1* gene causes reversion of the malignant phenotype (18–20). Although CEACAM1 is expressed in multiple isoforms with 1–4 Ig-like ectodomains and either long (72 amino acids) or short (12–14 amino acids) cytoplasmic domains, the short cytoplasmic domain isoforms predominate in epithelial cells. Because the cytoplasmic domain of this isoform is only 12–14 amino acids in length (the exact start of the domain is in doubt) it was originally thought not to play a role in signal transduction, but perhaps acted in a dominant negative fashion in the presence of the long cytoplasmic domain. However, we have shown that peptides or glutathione *S*-transferase fusion proteins from the short cytoplasmic domain bind directly to actin, tropomyosin, calmodulin, and more recently, to the annexin-2 p11 tetramer AIIt (21–23).

In this study, we have used mutational analysis of the short cytoplasmic domain of CEACAM1 to reveal which residues are involved in actin interactions and lumen formation. The results of our studies show that mutants F454A and K456A greatly decrease or increase, respectively, actin interactions, whereas the F454A and the double mutant T457A,S459A greatly reduce lumen formation. Further analysis reveals that either Thr^{457} or Ser^{459} are phosphorylated during lumen formation. The studies that identified these key residues are the subject of this report.

MATERIALS AND METHODS

Construction of Baits for Yeast Two-hybrid Screening

The nucleotide and amino acid sequence for CEACAM1–4S is taken from NCBI entry number NM_001712, gi:4502404, the full-length coding sequence including the N-terminal signal

* This work was supported by National Institutes of Health NCI Grant CA84202. The costs of publication of this article were defrayed in part by the payment of page charges. This article must therefore be hereby marked "*advertisement*" in accordance with 18 U.S.C. Section 1734 solely to indicate this fact.

[S] The on-line version of this article (available at http://www.jbc.org) contains supplemental Table S1.

[1] Both authors contributed equally to this research.

[2] Current address: Dept. of Experimental Oncology, Cross Cancer Institute, University of Alberta, Edmonton, Canada.

[3] To whom correspondence should be addressed: 1450 E. Duarte Rd., Duarte, CA 91010. Tel.: 626-359-8111 (ext. 62601); Fax: 626-301-8186; E-mail: jshively@coh.org.

[4] The abbreviations used are: CEACAM1–4S, carcinoembryonic antigen cell adhesion molecule 1, 4 ecto-domains, short cytoplasmic domain; CEACAM1–4L, carcinoembryonic antigen cell adhesion molecule 1, 4 ecto-domains, long cytoplasmic domain; CEA, carcinoembryonic antigen; STD, saturation transfer difference; EDC, *N*-ethyl-*N*′-(dimethylaminopropyl)-carbodimide hydrochloride; NHS, *N*-hydroxysuccinimide; Fmoc, *N*-(9-fluorenyl)methoxycarbonyl; HSQC, heteronuclear single quantum coherence; FBS, fetal bovine serum; eGFP, enhanced green fluorescent protein; MUA, mercaptoundecanoic acid; DBP, vitamin D-binding protein; TOCSY, total correlation spectroscopy.

sequence. To construct the bait containing the cytoplasmic domain of CEACAM1–4S (amino acids 451–464), pGKT7/CEACAM1–4S-cyt for yeast two-hybrid screening, an EcoRI site was introduced in front of Phe^{451} (nucleotide 1352) of CEACAM1–4S by site-directed mutagenesis, using a set of primers, 5′-GCAGTAGCCCTGGAATTCTTTCTGCATTTCG-3′/5′-CGAAATGCAGAAAGAATTCCAGGGCTACTGC-3′, and KS/CEACAM1–4S as template. The plasmid DNA was digested by EcoRI and PstI (located at 3′-untranslated region CEACAM1–4S cDNA). The resulting fragments were then subcloned into the pGKT7 (Clontech) between the EcoRI and PstI sites to create pGKT7/CEACAM1–4S-cyt. All PCR were performed using Pfu Turbo DNA polymerase (Stratagene, La Jolla, CA).

pGKT7/CEACAM1–4S-cyt Mutants

A series of single and dual alanine mutants of CEACAM1–4S-cyt were created by sequence overlap extension PCR. The Matchmaker 5′ DNA-BD vector insert screening sense amplimer was: 5′-TCATCGGAAGAGAGTAGTAAC-3′, and Matchmaker 3′ DNA-BD vector insert screening antisense amplimer was: 3′-GAGTCACTTTAAAATTTGTATAC-5′. For each mutant, a set of inside primers were synthesized (supplementary Table 1S). The pGKT7/CEACAM1–4S plasmid served as the template. In the first PCR run, the inside antisense primer was used with the external sense primer and the inside sense primer was used with external sense primer to create two overlapping fragments. Both of these fragments served as templates to produce the larger fragment using the external primer set. The resulting products were digested with EcoRI and PstI, and ligated into pGKT7 previously cut with the same restriction enzymes. The pGKT7/CEACAM1–4S-cyt was also mutated to create pGKT7/CEACAM1–4S-cyt-DD by site-directed mutagenesis using a set of primers (supplementary Table 1S). The amino acids mutated were T457D,S459D, which mimic phosphorylation at these two sites.

Yeast Two-hybrid Screen and Analysis

The Clontech human cDNA liver library used for screening contains 4×10^6 independent clones. The cytoplasmic domain from CEACAM1–4S (amino acids 451–464) was subcloned into pGKT7, transformed into yeast AH109 cells, and used as bait to screen the library. After mating, cells were plated on plates lacking Leu, Trp, His, and adenine (Ade). Colonies were replica plated onto a plate lacking Leu, Try, His, and Ade and printed onto a filter paper for β-galactosidase analysis using 5-bromo-4-chloro-3-indolyl-β-D-galactopyranoside (X-gal) as a substrate. Plasmid DNA of positive diploid clones were purified and transformed into *Escherichia coli* DH5. Transformants carrying the ACTII/prey were selected on LB/ampicillin plates. Plasmid DNA was purified and sequenced. The ACTII/prey plasmid DNA was transformed into yeast AH109 carrying the CEACAM1–4S-cyt bait construct or transformed into yeast Y187 for mating experiments. The co-transformants or mated cells were selected on plates lacking His and Trp. Colonies were picked and the supernatant of the overnight culture was used to assay for α-galactosidase. The cell mass was calculated by measuring the absorbance at $A_{600\,nm}$. The α-galactosidase activity was measured using *p*-nitrophenyl-α-galactopyranoside as a substrate according to the Clontech manual, and normalized to the cell mass ($A_{410/600\,nm}$) for comparison.

Mammalian Expression Vectors

To construct the mammalian expression vector pHβ-CEACAM1–4S-F454A, a single amino acid mutation (nucleotide 1360) was created by PCR site-directed mutagenesis, using KS/CEACAM1–4S as a template. KS/CEACAM1–4S-F454A was digested with SalI and HindIII and ligated into the pHβ-actin vector digested with SalI and HindIII. The β-actin promoter containing expression vector has been previously described (24).

pCDNA3/CEACAM1–4S-eGFP

To create a XmaI site for the insertion of eGFP into CEACAM1–4S, we first deleted the XmaI site located in the multicloning sites of the KS/CEACAM1–4S vector by PCR site-directed mutagenesis, using a set of primers: 5′-GAATTCCTGCAGCCTGGGGGGATCCACTAG-3′/5′-CTAGTGGATCCCCCAGGCTGCAGGAATTC-3′. An XmaI site was introduced between Pro^{427} (nucleotide 1279) and Gly^{428} (nucleotide 1281) of CEACAM1–4S by PCR site-directed mutagenesis, using the set of primers: 5′-GAAAATGGCCTCTCACCCGGGGCCATTGCTGGCATTG-3′/5′-CAATGCCAGCAATGGCCCCGGGTGAGAGGCCATTTTC-3′. A full-length eGFP clone containing a XmaI cutting site and a G4 linker on both ends was amplified by PCR using PE-GFP-N2 (Clontech) as the template, a set of primers containing XmaI site and the G4 linker, 5′-TCCCCCCGGGGGAGGAGGAATGGTGAGCAAGGGC-3′/5′-TCCCCCCGGGTCCTCCTCCCTTGTACAGCTCGTC-3′, were used. The PCR product was digested with XmaI, the eGFP fragment was purified and subcloned into KS (XmaI−)/CEACAM1–4S (XmaI+) previously digested with XmaI to create the KS/CEACAM1–4S-eGFP vector. The CEACAM1–4S-eGFP fragment was cut out from KS/CEACAM1–4S-eGFP and subcloned into pCDNA3 previously digested by KpnI and EcoRI. In the resulting vector a G4 linker were introduced after Pro^{427} of CEACAM1–4S, and a PG3 linker was introduced before Gly^{428} of CEACAM1–4S.

Mutations at Thr^{457} and Ser^{459} in the cytoplasmic domain of CEACAM1–4S were constructed according to the QuikChange Site-directed Mutagenesis Kit (Stratagene). In short, mutations were introduced into CEACAM1–4S/pBluescript II KS by PCR primers shown in supplementary Table 1S. PCR conditions were 95 °C for 1 min, 18 cycles at 95 °C for 30 s, 55 °C for 1 min, and 68 °C for 14 min. The parental (unmutated) strand was removed by DpnI digest. Mutants were sequenced and the selected clones were subcloned into the SalI and HindIII restriction sites of the pHβ-actin expression vector. Cell transfections were performed using Lipofectin reagent (Invitrogen) as per the manufacturer's instructions. Cells were maintained in minimal essential medium with 10% fetal bovine serum (FBS) and selected in 0.1–1.0 mg/ml G418 for 5 weeks to create stable CEACAM1–4S mutant cell lines. Geneticin-resistant cells were sorted for CEACAM1 expression, grown in a Matrigel sandwich assay, and scored for acinus formation. Statistical analysis was performed using Fisher's Exact test. For the

Matrigel sandwich assay, 12-well plates were coated with 150 μl of Matrigel and incubated at 37 °C for 30 min to let the Matrigel solidify. Cells (1×10^5) in 500 μl of mammary epithelial basal medium (MEBM) (Clonetics) plus pituitary gland extract (Cambrex) were added to each well. After 3 h of incubation the floating cells were removed and the bound cells were overlaid with 150 μl of 50% Matrigel (1:1, Matrgiel gel:MEBM plus pituitary gland extract and cholera toxin (100 ng/ml final)). Culture medium was changed every other day. After 6 days the Matrigel cultures were fixed with 2% paraformaldehyde or formaldehyde for histochemistry analysis.

Cell Culture and Transfection of Jurkat, HeLa, and MCF7 Cells

Jurkat cells were grown in RPMI supplemented with 10% FBS. MCF7 and HeLa cells were grown in Dulbecco's modified Eagle's medium supplemented with 10% FBS. Cells (1×10^7/ml) were harvested and washed in Opti-MEM. An aliquot (800 μl) of cell suspension was mixed with 25 μg of DNA (in 20–30 μl) and transferred to an electroporation cuvette with a 0.4-cm electrode gap (Bio-Rad). Electroporation parameters used were 260 V, 900 microfarads, resulting in a pulse time of 20–23 ms. Stable transformants were selected with geneticin and selected clones were shown to have high levels of cell surface expression by fluorescence-activated cell sorter and confocal fluorescence analysis. Cells were grown in Matrigel as described above.

Immunohistochemistry and Confocal Microscopy

Immunohistochemistry was performed according to Huang *et al.* (14) using anti-CEACAM1 monoclonal antibody 5F4 (kind gift from Dr. Richard Blumberg, Boston, MA). For immunofluorescence, Alexa 546 (Molecular Probes, Eugene, OR) conjugated monoclonal antibody T84.1 (1 μg/ml) was used to detect CEACAM1. Staining was visualized on a Zeiss model 310 confocal microscope. The cellular distribution of CEACAM1–4S in stably transfected Jurkat cells was performed on cells plated on 6-well slides precoated with 20 ng/ml fibronectin. Cells were incubated at 37 °C for 30 min followed by treatment with nocodazole (Sigma) or cytochalasin B (Sigma) at a final concentration of 5 μg/ml. After a 30-min incubation, cells were fixed in 2.5% paraformaldehyde in phosphate-buffered saline for 15 min and incubated for 1 h with anti-CEACAM1 antibody T84.1 (1:500), followed by a 1-h incubation with Alexa 488-conjugated goat anti-mouse IgG (Molecular Probes). After washing three times with cold phosphate-buffered saline, cells were permeabilized in PSG (0.01% saponinin phosphate-buffered saline) containing 0.5% Nonidet P-40 for 20 min at room temperature. Cells were stained for F-actin with Texas Red-conjugated phalloidin (Molecular Probes). For colocalization of CEACAM1–4S-eGFP with F-actin, Jurkat or MCF7 stable transfectants were grown in 6-well chamber slides in Dulbecco's modified Eagle's medium with 10% FBS. In some experiments chamber slides were precoated with laminin 10/11 (Sigma), followed by fixation and permeabilization as described above. F-actin was stained with Texas Red-conjugated phalloidin. The slides were mounted in 80% glycerol/phosphate-buffered saline and observed on a Zeiss confocal microscope using fluorescein isothiocyanate and rhodamine filter settings to detect GFP and Texas Red-phalloidin, respectively.

Peptide Synthesis

Synthetic peptides corresponding to the 12 amino acids adjacent to the transmembrane domain of the CEACAM1 short cytoplasmic domain were synthesized using Fmoc chemistry with an N-terminal mercaptoundecanoic acid (MUA) extension by the City of Hope Peptide Synthesis Core. ^{15}N-labeled Fmoc amino acids were purchased from Cambridge Isotope Labs. MUA was purchased from Aldrich, and the mercapto group was protected by reaction with trityl chloride. The *S*-trityl derivative was purified by silica gel chromatography. Briefly, 11-mercaptoundecanoic acid (10 mmol, 2.18 g) was dissolved in dry pyridine (20 ml) and trityl chloride (11 mmol, 3.06 g) was added. The reaction mixture was left for 18 h, quenched with 20 ml of ethanol, and concentrated under reduced pressure. The residue was dissolved in 150 ml of dichloromethane, cooled to 0 °C, and washed with ice-cold 1 M citric acid (3 × 50 ml) and saturated brine (50 ml), dried with anhydrous magnesium sulfate, and concentrated under reduced pressure. The crude product was purified on Silica Gel H (120 g) in a gradient of ethanol/dichloromethane (0–3%) with 1% of acetic acid present in both. Chromatography was monitored by TLC (Si60, Merck) in 10% dichloromethane/ethanol/acetic acid (89:10:1). The yield of pure product (R_F = 0.65) was 4.0 g (8.75 mmol). Trityl-S-MUA (0.25 mmol) was dissolved in 0.5 ml of 1-methyl-2-pyrrolidinone, 0.5 M HOBt, and reacted with 0.25 ml of 1 M dicyclohexylcarbodiimide in dichloromethane for 30 min, filtered to remove the precipitated urea, and added to the peptide/solid support (0.1 mmol) containing a free amino group. Coupling was performed at 65 °C for 30 min, the resin was washed with *N*,*N*-dimethylformamide, dichloromethane, dried, and cleaved with trifluoroacetic acid/water/ethanethiol/triethylsilane (90:5:2.5:2.5) for 30 min at 40 °C. Peptides were purified to >95% purity by reversed-phase high performance liquid chromatography on a Vydac C_{18} column and their masses confirmed by electrospray ionization mass spectrometry on a Finnigan LCQ ion trap mass spectrometer.

BIAcore Analysis

Biomolecular interaction analyses were carried out in HBS buffer (150 mM NaCl, 0.05% (v/v) Surfactant P20, 10 mM HEPES, pH 7.4 or 5.5) using the BIAcore® 2000 (BIAcore, Inc.). Depending on the experiment, 2 mM $CaCl_2$ was added to the HBS. Nonmuscle G-actin (Cytoskeleton, Inc.) was immobilized on a CM5 sensorchip (BIAcore) using the Amine Coupling Kit (BIAcore). The surface of the sensorchip was activated with 30 μl of EDC/NHS (100 mM *N*-ethyl-*N*′-(dimethylamino-propyl)-carbodimide hydrochloride, 400 mM *N*-hydroxysuccinimide) using a flow rate of 5 μl/min. For immobilization of proteins, 1–10 μg of G-actin or vitamin D-binding protein (DBP, Sigma) in 100 μl of 10 mM sodium acetate, pH 4.0, were applied (flow rate: 5 μl/min). Subsequently, the sensorchip was deactivated with 30 μl of 1 M ethanolamine hydrochloride, pH 8.5 (flow rate: 5 μl/min), and conditioned with 10 μl of 25 mM HCl (flow rate: 20 μl/min). Thiol immobilization of MUA peptides was performed according to application note 9 from BIAcore. Briefly, a

CM5 chip was activated by NHS/EDC (1:1, 10 μl) followed by pyridine disulfide ethane amine (20 μl of 80 mM in 0.1 M sodium borate, pH 8.5) followed by MUA-peptide (7.5 μl of 2 mg/ml in 10 mM sodium acetate, pH 4.0) followed by cysteine, 1 M NaCl (20 μl of 50 mM in 0.1 M sodium acetate, pH 4.0) to block excess sites. Binding studies and regeneration of the chip surface between injections were carried out at a flow rate of 20 μl/min unless otherwise noted. Samples were diluted in HBS buffer immediately prior to injection. Between sample injections the surface was regenerated with 15 μl of 25 mM HCl. Data were analyzed with BIAevaluation 3.1 software (BIAcore), and curve fitting was done with the assumption of one-to-one (Langmuir) binding.

NMR Analysis

HSQC—Peptide solutions were prepared by dissolving lyophilized powders in 5 mM Tris buffer containing 5% D_2O, 0.1 mM $CaCl_2$, 0.2 mM ATP, and dithiothreitol (G-buffer, Cytoskeleton, Inc.) and the pH adjusted to 5.4 with 0.1 M HCl. The concentrations of wild-type and F454A mutant peptide were 0.10 and 0.15 mM, respectively. Actin was added to the peptide by dissolving lyophilized actin (Cytoskeleton, Inc.) in the peptide solution and the pH adjusted as necessary. The two-dimensional ^{1}H-^{15}N correlated HSQC experiments were carried out on a Bruker Avance 600 NMR instrument equipped with actively shielded Z-gradient TXI-triple resonance cryoprobe. The Watergate-HSQC with water flip-back pulse was used for water suppression. The experiments were carried out at 15 °C.

STD (Saturation Transfer Difference)—Experiments are widely used to identify the interaction between small ligand and large target biomolecules, and to determine the binding epitope of the ligand (25, 26). The advantage of the STD approach is that it works on large sized, and low concentrations of biomolecules without a requirement for isotope labeling of biomolecules. The concentration of protein can be as low as in the nanomolar range, and the optimal K_D ranges from 10^{-3} to 10^{-8} M. STD is composed of two experiments. The first is a saturation experiment with carrier frequency irradiation on protein signals for a period of 2–5 s with soft pulse so that the target signals are saturated and ligand signals are not excited. Next, a reference experiment is carried out with a carrier frequency far away from protein and ligand signals. The two experiments are usually carried out in an interleaved fashion and the subtraction is realized by phase cycling. For a large sized protein, the saturation on any part of the protein (usually the methyl region) is spread out quickly through a spin diffusion mechanism to whole protein as well as the ligand in close contact with the protein. The protein signals from the subtraction of two experiments can be removed by a spin-lock delay (typically 40 ms), and thus the surviving signals are from the ligand that interacts with protein. Furthermore, epitope binding information can be obtained from the intensity of STD signals.

STD experiments were performed according to Mayer and Mayer (25). Rabbit muscle actin (1 mg) was dissolved in 2 ml of G buffer, and then dialyzed two times *versus* 1 liter of G buffer at 4 °C. After dialysis, the G buffer was extensive exchanged to a G buffer prepared with D_2O, deuterated dithiothreitol, and deuterated Tris. The final actin concentration was about 0.02 mM. STD experiments were carried out on a 500 MHz Bruker instrument with a TXI probe equipped with triple axis gradients. The irradiation power of the selective Gauss-shaped pulses was set to 86 Hz with duration of 55 ms. Saturation of actin signals was achieved with a train of 70 gauss-shaped pulses separated by a 1-ms delay. The on-resonance irradiation of the actin sample was carried out at −2.4 ppm, and no saturation of CEACAM1 peptide in the absence of actin was observed under these experimental conditions. The off-resonance irradiation was performed at −30 ppm. A 40-ms spin-lock pulse with field strength of 4960 Hz was used to suppress the background signals of actin. The saturation time was optimized by arraying the numbers of gauss-shaped pulse, and the highest STD signals were obtained with saturation time of 3.9 s.

Molecular Modeling—A molecular model of CEACAM1–4S transmembrane and cytoplasmic domains was built using the HOMOLOGY module within INSIGHT II 2000 software (Accelrys Inc., San Diego, CA). Predicted transmembrane residues 429–452 were modeled using residues 437–460 from the membrane protein AcrB multidrug efflux pump as a template (26). Coordinates for the cytoplasmic tail (residues 453–464) were modeled using residues 132–143 of the DBP bound to actin as a template (27). The DBP-actin complex also served as a template for the initial docking of the cytoplasmic domain of CEACAM1–4S with the terminal unit of F-actin, as modeled by Holmes *et al.* (28), coordinates were courtesy of Ken Holmes, Max Planck Institute for Medical Research, Heidelberg, Germany. To complete the model, the transmembrane helix of CEACAM1–4S was embedded in a standard model of a fluid lipid bilayer. Docking was optimized using the DISCOVER 3.0 module within INSIGHT II. The consistent valence force field was used throughout (29). The conformation of the cytoplasmic domain of CEACAM1–4S and segments of actin within 4.5 Å were simultaneously optimized using molecular dynamics (50 ps at 300 K) followed by conjugate gradient minimization to a maximum derivative of 0.5 kcal/mol Å.

Phosphorylation of CEACAM1–4S—MCF7 cells (1×10^7) transfected with CEACAM1–4S were grown in a three-dimensional culture for 4 days, incubated with phosphate-free RPMI 1640 plus 1% dialyzed FBS and 11 mCi of [^{32}P]orthophosphate (ICN), harvested with Matrisperse (Collaborative Biomedical Products), and lysed with 2% Nonidet P-40. CEACAM1 was immunoprecipitated with anti-CEACAM1 monoclonal antibody T84.1, and the proteins separated by SDS-gel electrophoresis and Western blot and autoradiography was performed to locate the ^{32}P-labeled CEACAM1 band. The band was excised and counted in a Packard 1600CA scintillation counter. In a second experiment for CEACAM1–4S, transfected and vector control cells were grown for 4 days in Matrigel, harvested with Matrisperse, and lysed with 2% Nonidet P-40. CEACAM1 was immunoprecipitated as above and Western blot analysis was performed with anti-CEACAM1 monoclonal antibody T84.1, polyclonal antibody 22-9 that is specific for the cytoplasmic domain of the short cytoplasmic domain of CEACAM1, or phospho-Ser phospho-Thr-specific antibodies (Calbiochem).

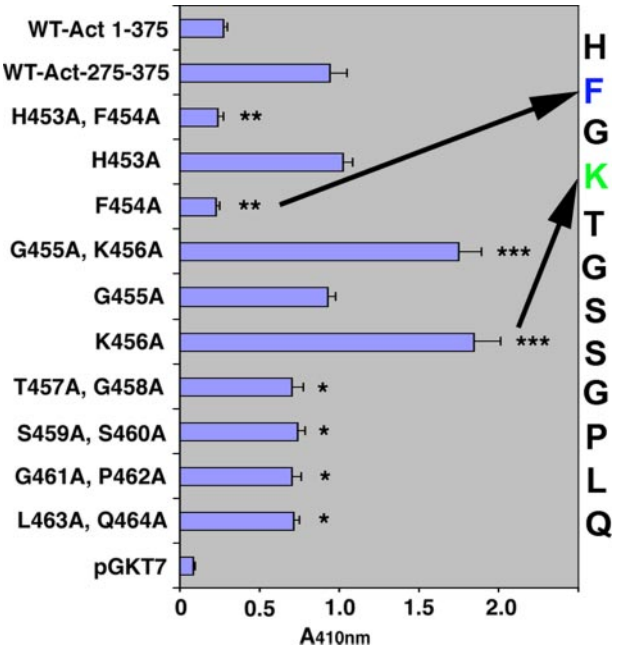

FIGURE 1. **Identification of the actin interaction regions in the CEACAM1–4S cytoplasmic domain by a quantitative yeast two-hybrid assay.** The sequence of the cytoplasmic domain is shown to the *right*. CEACAM1–4S-cyt wild-type and mutant constructs were inserted into vector pGKT-7 and β-actin C-terminal domain constructs into ACTII. Each mutant construct was co-transformed into yeast Y187 with ACTII/β-actin. The strength of interaction of each construct with a partial clone of β-actin-(275–375) was quantified by α-galactosidase solution phase assay in quadruplicate as described under "Materials and Methods." Empty vector pGKT7 was used as a negative control. *p* values were calculated by a χ-squared test (*, <0.002; **, $<10^{-5}$; ***, $<10^{-6}$).

RESULTS AND DISCUSSION

Identification of Actin Binding Residues by a Yeast Two-hybrid Assay—To identify the cytoplasmic domain residues in CEACAM1–4S that can interact with actin *in vivo*, we exploited the power of the yeast two-hybrid assay. The assay was first validated by an unbiased screen of a 14-amino acid version of the cytoplasmic domain of CEACAM1–4S (see Fig. 1) as bait *versus* a human liver cDNA library fused to the Gal4 AD (pACTII vector) as prey. A liver cDNA library was chosen because of the high level of polarized expression of CEACAM1 and its co-localization with actin in hepatocytes (1). Of 4.2×10^6 yeast transformants, more than 3000 positive clones were obtained of which 50 were randomly selected for sequence analysis. Only 10 of the 50 clones had an in-frame coding sequence. Two of these clones corresponded to the C-terminal region of β-actin (residues 275–375). As expected for this type of library, the β-actin clones were not full-length. However, the fact that the bait bound to the C-terminal region of β-actin suggested the possibility that the binding site was in the C-terminal region (subdomains 1 and 3) that encompasses a hot spot where multiple actin-binding proteins bind, including DBP, marine toxins, ADF/cofilin, gelsolin, and F-actin (30).

To determine critical residues in the cytoplasmic domain bait, the relative strengths of interaction of various mutants were determined using α-galactosidase as the inducible marker. When the β-actin prey (pACTII/β-actin-275–375) was co-transformed into cells with the empty bait vector, no significant α-galactosidase activity was detected. However, when the cells were co-transformed with the CEACAM1–4S-cyt bait significant α-galactosidase activity was observed (Fig. 1), indicating that the bait-prey interaction was specific. Because the partial actin clone contained only a C-terminal portion of β-actin, we also generated a full-length β-actin construct (pACTII/β-actin-(1–375)) that also interacted with the CEACAM1–4S-cyt bait, but at a lower relative strength (Fig. 1). This result suggested that the β-actin binding site for the cytoplasmic domain of CEACAM1–4S may be less accessible or inherently weaker in the full-length *versus* the C-terminal partial clone of β-actin. Although the magnitude of binding was uniformly lower, the binding orders of various mutants were the same when comparing different full-length *versus* partial clones of β-actin as prey.

To further define the interacting sites of the cytoplasmic domain of CEACAM1–4S with β-actin, six double Ala mutants of CEACAM1–4S-cyt were tested against the C-terminal clone of β-actin because of its higher response in the α-galactosidase assay compared with the full-length clone. When residues His^{453} and Phe^{454} were replaced by Ala, the binding activity was decreased to 25% of the parental wild-type construct (Fig. 1). When the following two residues were replaced with Ala (G455A,K456A) a 40% increase in binding was observed. All of the subsequent double Ala mutants did not show a dramatic effect on binding activity. To define the role of individual residues in the critical sequence HFKG, single Ala mutants were constructed at each residue and the binding activity of each construct measured. The F454A mutant had the same degree of inhibition of actin binding as the double mutant (H453A,F454A), whereas the H453A mutant had the same β-actin binding activity as the wild-type construct. Similarly, analysis of single alanine mutants demonstrated that replacement of Lys^{456} with Ala was responsible for the increase in binding activity observed with the double mutant. These results indicate that Phe^{454} and Lys^{456} play major roles in mediating the direct interaction of the CEACAM1–4S cytoplasmic domain with β-actin, one residue exerting a positive effect on binding, and the other exerting a negative effect on binding.

A Membrane Model of the CEACAM1 Cytoplasmic Domain Interaction with Actin—Although we have demonstrated that the 12–14-amino acid cytoplasmic domain of CEACAM1–4S can directly interact with actin, tropomyosin, calmodulin, and more recently, with AIIt (the annexin 2-p11 tetramer), the short length of the cytoplasmic domain, the controversy over its exact start, and its close proximity to the membrane create difficulties in conceptualizing these interactions. In fact, most physical measurements of its molecular interactions have involved glutathione *S*-transferase fusion proteins or peptides immobilized on biosensor chips, ignoring the proximal effects of the transmembrane domain and lipid bilayer (21). To understand these effects better, a model with the transmembrane domain traversing a lipid bilayer was constructed and both an actin monomer and F-actin filament were docked to the cytoplasmic domain using all of the available information from the yeast two-hybrid experiments. Because the C-terminal 100 amino acids of actin corresponds mostly to subdomain 3, we constructed a model in which CEACAM1–4S binds this subdomain. Potential docking sites were identified by examining

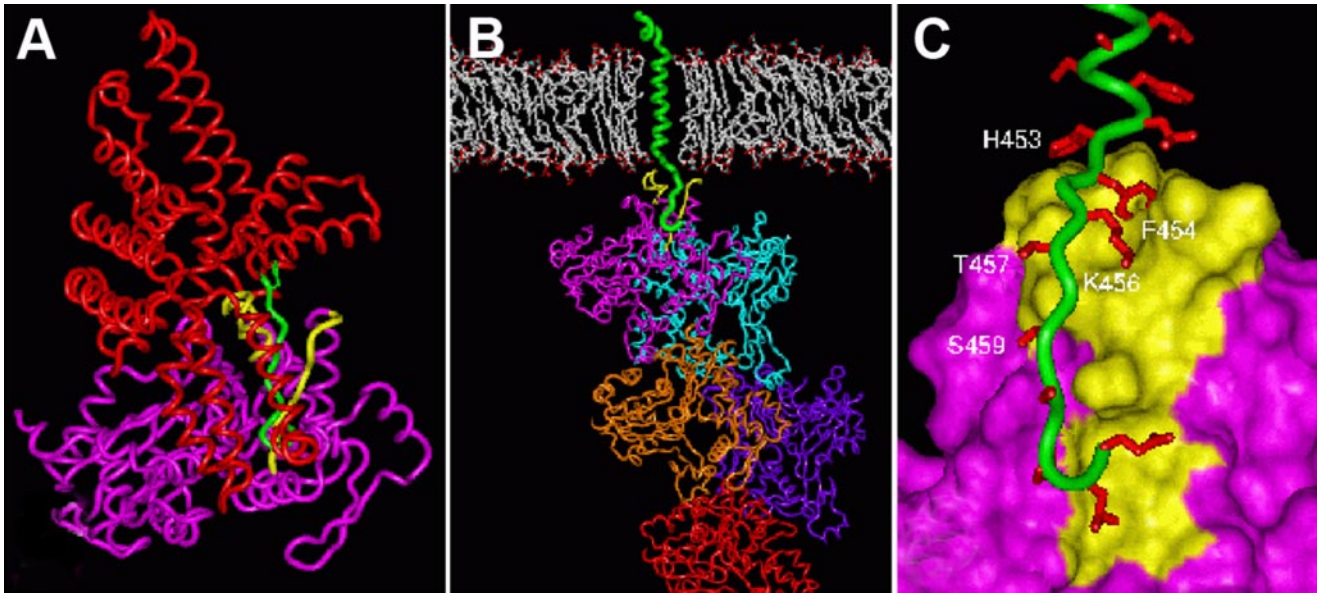

FIGURE 2. **A membrane model for the interaction of actin with the CEACAM1–4S cytoplasmic domain.** *A*, ribbon rendering of modeling template vitamin D-binding protein (*red*) interacting with rabbit actin (*magenta* and *yellow*). Segment 133–143, which served as a template for modeling CEACAM1–4S, is highlighted in *green*. The side chain Phe[133] that docks in the actin groove is also shown. *B*, ribbon model of transmembrane and cytoplasmic domains of CEACAM1–4S (*green*) interacting with F-actin (5 G-actin units colored *magenta*, *cyan*, *orange*, *purple*, and *red*). The transmembrane helix of CEACAM1–4S is embedded in a previously published phospholipid bilayer model (39, 40). Actin segments 281–292 and 323–332 in the terminal unit are highlighted (*yellow*). *C*, close-up view of CEACAM1–4S-actin interaction, showing His[453] at the end of the transmembrane helix and Phe[454] buried at the head of a surface groove formed by actin segments 281–292 and 323–332.

all published crystal structures of actin bound to various proteins, peptides, and small molecules. Using this information, DBP bound to actin (27) was identified as the most suitable modeling template, not only because it binds to subdomain 3, but also because the interaction involves a linear stretch of amino acids (DBP residues 133–143) that begins with a phenylalanine (Fig. 2*A*). Assuming an α-helix for the transmembrane portion of CEACAM1–4S, the last amino acid in contact with the phospholipid portion of the lipid bilayer is probably His[453], a residue that may be positively charged, helping to anchor the transmembrane domain and orient the cytoplasmic domain. Interestingly, the next residue, Phe[454], and those that follow, are in positions to make a docking contact with either G- or the terminal unit of F-actin (Fig. 2*B*) in a groove defined by segments 281–292 and 323–332 (Fig. 2*C*). Granted, the DBP-actin interaction buries a much larger surface area and involves several discontinuous peptide segments rather than a single short peptide extending from a membrane as we have modeled, but the template underscores the possibility that this particular groove on actin can utilize Phe as a docking residue in its interactions with other proteins. Therefore this model is consistent with our conclusion from the yeast two-hybrid studies that indicated Phe[454] was a critical residue. It is also important to note that segments 281–292 and 323–332 contribute residues to loops that supposedly participate in actin-actin interactions when G-actin polymerizes to form F-actin (31, 32), thus underscoring the fact that these segments constitute a widely utilized multifunctional binding site. This observation may also explain why actin fragment 275–375 was much more active in our yeast two-hybrid assay than whole actin. The latter has the potential to undergo polymerization, thus masking many potential CEACAM1–4S binding sites, whereas the former does not. Furthermore, actin fragment 275–375 probably dimerizes because many previously buried hydrophobic residues are exposed when the fragment is expressed in isolation. Dimerization would be expected to increase the avidity of the prey compared with native actin.

Binding Kinetics of the Cytoplasmic Domain-Actin Interactions—To test the role of Phe[454] in CEACAM1–4S in a kinetic assay, we immobilized actin on a CM5 BIAcore chip and tested the binding of the wild-type synthetic peptide *versus* the F454A mutant. Previous studies had shown that the cytoplasmic domain peptide expressed as a glutathione *S*-transferase fusion protein bound to immobilized actin with a K_D of 30 nM, whereas the actin co-sedimentation assay gave a K_D of 7 μM (21). However, both of these assays fail to mimic the *in vivo* situation where the cytoplasmic domain protrudes from the phospholipid membrane in an organized, oriented manner. To approximate these conditions, we have synthesized the CEACAM1 cytoplasmic domain peptide with an N-terminal MUA acyl group that permits oriented binding of the peptide to a biosensor gold surface (23), in solution as oriented micelles, or as described later, to a CM5 chip using thiol immobilization chemistry. As show in Fig. 3*A*, the wild-type *N*-acyl MUA peptide binds to immobilized actin with a K_D of 2.94 μM, a result in reasonable agreement with our co-sedimentation study. Moreover, when the F454A mutated *N*-acyl MUA peptide was tested, no binding was detected (Fig. 3*A*), a result in agreement with our membrane model and yeast two-hybrid results. Because the actin-binding protein DBP was used in our membrane model, we also tested its ability to bind actin under the same assay conditions (Fig. 3*B*). Surprisingly, no DBP binding to immobilized actin was observed, but when DBP and wild-type *N*-acyl MUA peptide were mixed, increased binding was seen over that

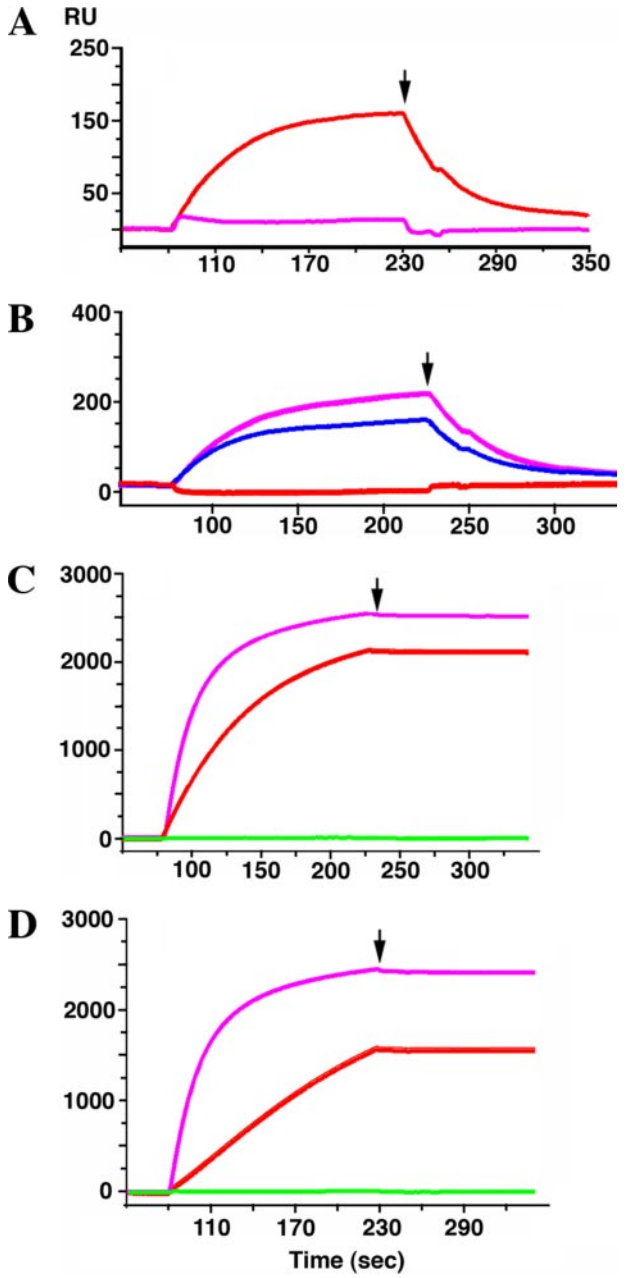

FIGURE 3. **Effect of F454A mutation of the cytoplasmic domain of CEACAM1–4S on actin binding.** BIAcore binding experiments were performed on CM5 chips using HBS in the absence of 2 mM $CaCl_2$ at pH 7.0. *A*, actin immobilized on a CM5 chip binds wild type but not mutant peptide. *Upper curve*, binding of 2.5 μM wild-type *N*-acyl MUA-peptide; *lower curve*, binding of 2.5 μM F454A *N*-acyl MUA-mutant peptide. *B*, actin immobilized on a CM5 chip does not bind DBP. *Upper curve*, 2.5 μM wild-type *N*-acyl MUA-peptide + 0.17 μM DBP; *middle curve*, 2.5 μM wild-type *N*-acyl MUA-peptide; *lower curve*, 0.17 μM DBP. *C*, DBP immobilized on a CM5 chip binds actin. *Upper curve*, 0.84 μM actin; *middle curve*, 0.84 μM actin + 2.5 μM wild-type *N*-acyl MUA-peptide; *lower curve*, 2.5 μM wild-type *N*-acyl MUA-peptide. *D*, wild-type *N*-acyl MUA-peptide immobilized by amine chemistry on a CM5 chip binds actin. *Upper curve*, 0.84 μM actin; *middle curve*, 0.84 μM actin + 0.1 μM DBP; *lower curve*, 0.1 μM DBP. *RU*, resonance units.

of peptide alone. This means that the peptide was able to promote DBP binding to actin, suggesting that actin undergoes a state change upon interaction with peptide. The inability of DBP to bind immobilized actin prompted us to test the system in the opposite configuration, where DBP is immobilized and actin is passed over the chip. In this case, actin binds to immobilized DBP showing saturable binding with negligible dissociation. As expected, the wild-type *N*-acyl MUA peptide shows no DBP binding (Fig. 3*C*). However, when actin is mixed with the peptide, inhibition of binding is observed, suggesting that the two share an overlapping actin-binding site, as predicted by our model.

The asymmetric BIAcore binding results obtained with DBP and actin were also observed for the N-acyl MUA peptide and actin, but in the opposite manner. When actin is passed over either thiol-immobilized *N*-acyl MUA peptide on a CM5 chip or immobilized on a bare gold surface, no binding is observed (data not shown). However, if the *N*-acyl MUA peptide is immobilized by amine chemistry (binding through Lys^{456}) to a CM5 chip, saturable binding is observed with negligible dissociation (Fig. 3*D*). When actin is mixed with DBP, inhibition of binding is observed (Fig. 3*D*), demonstrating again that DBP and peptide compete for the same binding site, as our model predicts. Thus, both the yeast two-hybrid and biochemical studies demonstrate the binding of the cytoplasmic domain of CEACAM1–4S to actin and provide evidence that Phe^{454} is a critical residue.

Binding of the Cytoplasmic Domain to Actin Demonstrated by NMR HSQC and STD Studies—The asymmetric binding of the CEACAM1 *N*-acyl MUA peptide to actin suggests that actin binding is controlled by either a conformational change in actin, in the peptide, or in both actin and the peptide. To further explore this idea, we synthesized the wild-type peptide incorporating ^{15}N-Phe in the position of Phe^{454}, with the expectation that the ^{15}N-^{1}H correlated peak would be shifted in the presence of actin. Surprisingly, no HSQC cross-peak was observed for this peptide at pH 7.0, even in the absence of actin. However, when an ^{15}N natural abundance spectrum was recorded using a much higher peptide concentration (20 mM), signals were observed for all other amide protons in the peptide (data not shown). To explain these results, the amide proton at Phe^{454} must be completely dissociated or line broadened to baseline levels at pH 7. When the pH was lowered to 5.5, the HSQC cross-peak appeared (Fig. 4*A*), in support of the idea that this amide proton is completely dissociated at pH 7.0. In addition, the HSQC cross-peak was significantly shifted by the addition of actin (Fig. 4*A*), demonstrating the interaction of Phe^{454} with actin. When the experiment was repeated with the mutated ^{15}N-labeled F454A peptide, only a minor shift was observed on the addition of actin (Fig. 4*B*). Upon examination of the peptide sequence, we predicted that the peptide might undergo a β or γ turn at residues 454–456 (Phe-Gly-Lys) and that the ϵ-amino group of Lys^{456} is the best candidate group responsible for the deprotonation of the Phe^{454} backbone amide at pH 7, most likely via stabilization of the enol form of the amide. The prediction that Lys^{456} plays a role in actin binding is supported by the yeast two-hybrid results that show that the K456A mutant has increased actin binding over the wild-type sequence.

To further confirm the interaction between the peptide and actin, STD experiments (see "Materials and Methods" for an explanation of the technique) were performed on both wild-type and F454A peptide at pH 7 according to Mayer and Meyer (25). The molar ratios between both peptides and actin were 100:1 with actin concentrations of 0.02 mM. Other experimen-

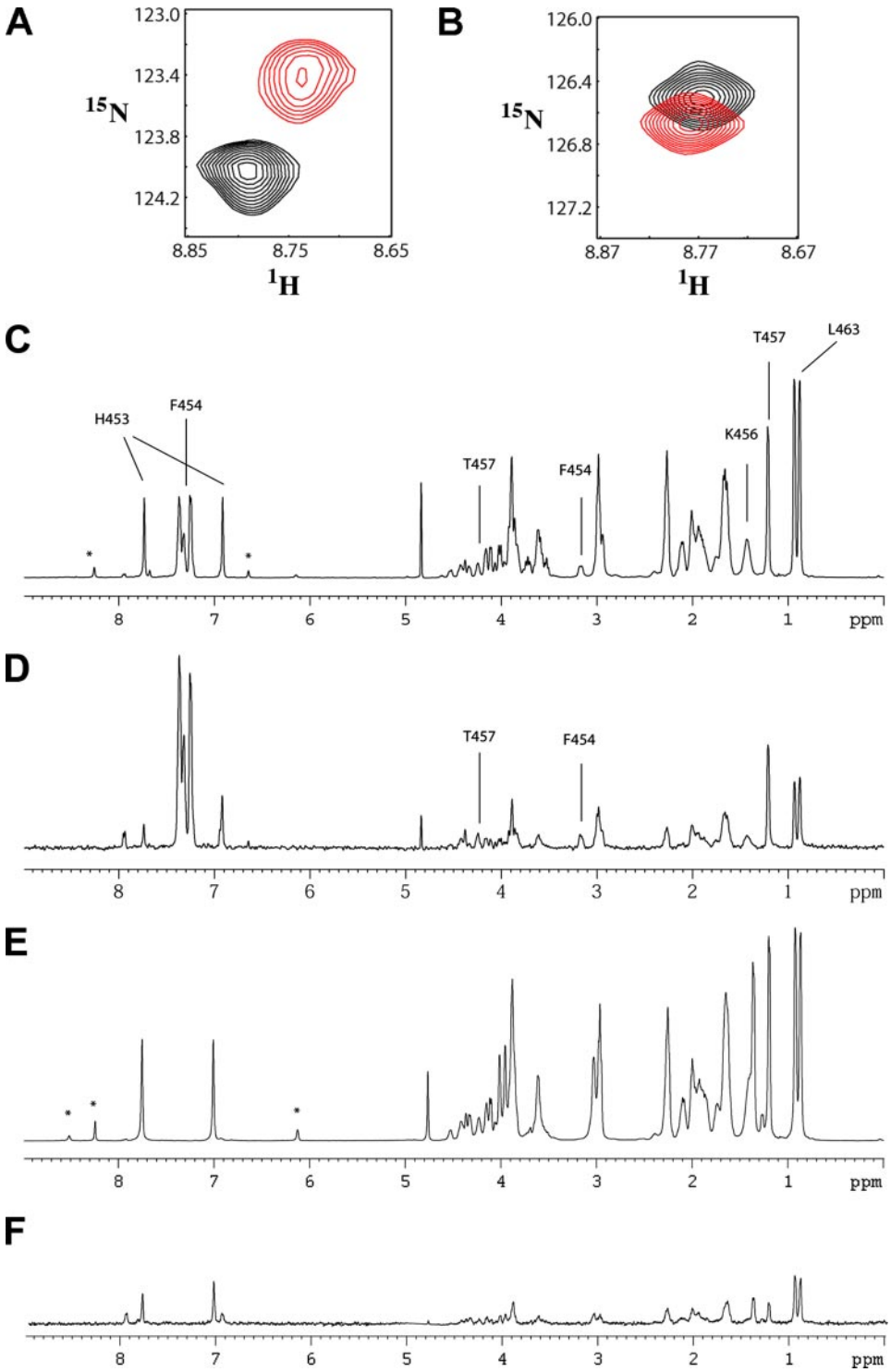

FIGURE 4. **Interaction of CEACAM1 short cytoplasmic domain peptide using HSQC and STD NMR.** *A*, ^{1}H-^{15}N correlated HSQC spectra for the titration of the ^{15}N-F454-labeled peptide with actin. The concentration of peptide was 0.1 mM in 5 mM Tris-HCl, pH 5.4, 0.1 mM $CaCl_2$, 0.2 mM ATP, 0.2 mM dithiothreitol. The concentration of actin was 0 and 0.1 mM for the *black* and *red* cross-peaks, respectively. The spectral widths for ^{1}H and ^{15}N were 8389 and 608 Hz, respectively, with acquisition points of 1024 and 64, respectively. The size of the data matrix after Fourier transformation was 2048 × 256, with a digital resolution of 0.01 and 0.04 ppm for ^{1}H and ^{15}N dimensions, respectively. *B*, ^{1}H-^{15}N-correlated HSQC spectra for the titration of ^{15}N-A454-labeled peptide with actin. The concentration of peptide was 0.11 mM. The concentration of actin was 0 and 0.15 mM for the *black* and *red* cross-peaks, respectively. The spectrum parameters were the same as above. *C* and *D*, one-dimensional ^{1}H spectra of STD reference (*C*) and STD (*D*) acquired using standard one-dimensional STD with 3-9-19 watergate on the actin/wild-type peptide complex samples dissolved in G buffer prepared with D_2O. The molar ratio of actin:peptide is 1:100. The experiments were carried out at 25 °C with the same receiver gain. The spectral width is 16 ppm. The number of scans for *C* and *D* are 64 and 1280, respectively. The same Lorentzian line-broadening of 0.3 Hz was applied to the two experiments for data processing. The peak integrations and the extraction of relative peak intensity between two experiments were carefully carried out with Bruker Xwinnmr software. Other experimental parameters are described under "Materials and Methods." Some well resolved peaks are labeled in *C* and *D*. The peaks with an *asterisk* are from ATP. *E* and *F* are the one-dimensional ^{1}H spectra of STD reference (*E*) and STD (*F*) acquired on the F454A mutant peptide-actin complex dissolved in G-buffer prepared with D_2O. The number of scans for *E* and *F* are 64 and 2048, respectively. The same Lorentzian line broadening of 2 Hz was applied to the two experiments for data processing. The other experimental conditions are the same as described above for *C* and *D*.

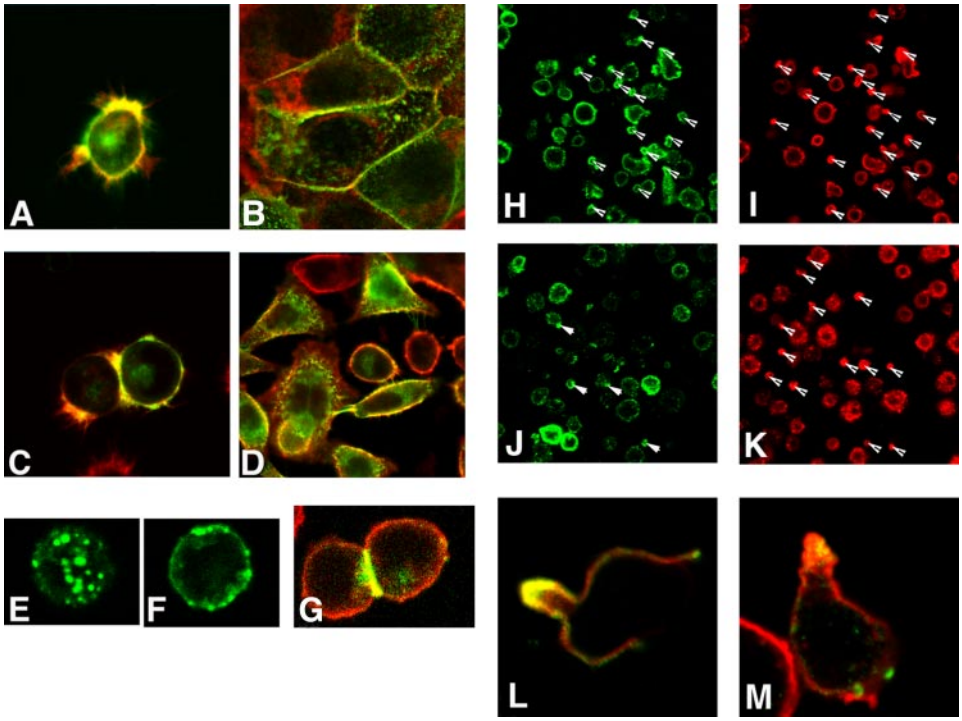

FIGURE 5. **Co-localization of CEACAM1–4S-eGFP with F-actin and effect of F454A mutation on cytoskeletal rearrangements in transfected Jurkat cells.** CEACAM1–4S-eGFP-transfected MCF7 cells were grown on laminin coated (*A*) or plastic (*B*) slides, permeabilized, stained with Texas Red-phalloidin and analyzed by confocal microscopy. Only merged images are shown. CEACAM1–4S-eGFP HeLa-transfected cells were grown on laminin coated (*C*) or plastic (*D*) slides and stained as above. CEACAM1–4S-eGFP transfected Jurkat cells were grown on fibronectin-coated slides and *z* sections taken at the top (*E*) and center (*F*) of the cells. Only the *green* channel is shown. Cells were permeabilized and stained with Texas Red-phalloidin (*G*). Only the merged image is shown. CEACAM1–4S-eGFP Jurkat transfectants were grown on fibronectin-coated slides and treated with 5 μg/ml nocodazole for 2 h. The cells were permeabilized and stained with Texas Red-phalloidin, and both *green* and *red* fluorescent channels recorded. *H* and *I*, *green* (CEACAM1) and *red* (phalloidin) channels for Jurkat cells transfected with wild-type CEACAM1–4S-eGFP. *Arrows* indicate substrate-attached blebs. *J* and *K*, *green* and *red* channels for Jurkat cells transfected with F454A mutant. *Arrows* indicate substrate-attached blebs. When multiple fields were counted, the average number of co-localized blebs for the wild-type transfectants was ~80%, whereas for the F454A mutant transfectants was about 30%. *L* and *M*, a *z*-section near the plane of the slide showing *green-red* merged images for the wild-type (*L*) and F454A mutants (*M*). Note: the majority of green fluorescence is out of the plane for this *z*-section.

tal conditions are described in the figure legends. The ^{1}H one-dimensional NMR assignments were based on the two-dimensional natural abundance ^{1}H-^{13}C HSQC and HSQC-TOCSY spectra acquired on the free peptides. Fig. 4, *C* and *D*, are the reference and STD experiments on wild-type peptide complexed with actin. Strong STD signals observed from residues Phe^{454} and Thr^{457} indicate these two residues are in close contact with the surface of actin. The highest STD signals are from H3,5, H4 (41%) followed by H2,6 (35.8%) of Phe^{454}. The STD signals are 14.6, 11.5, and 13.0% for Hβ and Hγ of Thr^{457}, Hβ of Phe^{454}, respectively. All other well resolved STD signals are in the 2.9 to 6.7% range. The STD signal of Hγ from Lys^{456} is 4.9, which means that Lys^{456} is not in close contact with actin, but may play a regulatory role in the interaction between peptide and actin as discussed in the last section. Because the strongest STD signals are observed for all five protons on the aromatic ring of Phe^{454}, the results are in agreement with the model that shows the aromatic ring embedded in a hydrophobic pocket in actin. Signal H4 of His^{453} is superimposed on either an impurity or minor conformation of the peptide making analysis of its interaction with actin difficult to interpret. Even including these contributions, the STD of H4 of His^{453} is only 15%. In agreement, the STD for H1 of His^{453} is even less (5.6%). The ATP signals marked with an asterisk did not appear in the STD spectra because ATP binding to actin is tight ($K_D \sim 7 \times 10^{-11}$ M) (27). Although several impurity or minor peptide conformation signals (less than 5% in the reference spectra) are present in the STD spectra, they do not interfere in the analysis, except for H4 of His^{453} as discussed above. Fig. 4, *E* and *F*, show the reference and STD experiments carried out on the mutant F454A peptide in complex with actin. Compared with the wild-type peptide, the overall STD signal intensity is much less than the STD values observed on the wild-type peptide-actin complex. The maximum STD of the mutant peptide is only 2.5% from Leu^{463} methyl group. All other well resolved peaks have STD signals in the range from 0.5 to 1.1%. These insignificant STD signals indicate that mutant peptide has no specific interaction with actin. Thus, the STD data confirm that the wild-type but not the F454A mutant peptide interacts with actin under physiological conditions.

Confocal Analysis of Wild-type and Mutant CEACAM1–4S-Actin Interactions—To test the role of Phe^{454} of CEACAM1–4S *in vivo*, we used live cell transfection assays and examined the co-localization of mutant CEACAM1–4S-eGFP fusion proteins with actin. Because we wanted to avoid affecting either the cell-cell adhesion properties of CEACAM1 that are contained in the N-terminal domain (33) or the signaling activities contained in the short cytoplasmic domain, the *eGFP* gene was inserted just prior to the start of the transmembrane domain. Previously, we have shown that this fusion protein is expressed at the plasma membrane and faithfully executes a morphogenic program in the three-dimensional culture of transfected MCF7 cells (16). In all cases, clones were selected based on their high level of surface expression of the transfected gene. When the MCF7/CEACAM1–4S-eGFP transfectants were grown on laminin-coated slides and stained with phalloidin for F-actin, the laminin attachment areas revealed a halo of co-localized β-actin and CEACAM1–4S extended beyond the cell perimeter (Fig. 5*A*). In this case, the cells have just begun to flatten out after attachment to substrate. The results show a uniform expression of CEACAM1–4S on the cell surface, but demonstrate that F-actin and the fusion protein have concentrated to the newly forming lamellapodia and fillopodia. Notably, CEACAM1–4S co-localizes to all but a few of the F-actin attachment points, which in some cases exclude CEACAM1. Because integrins play a

major role in the attachment points, these results may suggest that CEACAM1 involvement is limited to a subset of integrins in agreement with our previous studies (34). When the same cells are grown on plastic, they exhibit a typical epithelial cell morphology and demonstrate CEACAM1–4S and F-actin enrichment and co-localization between the cells (Fig. 5*B*). This result is typical of the staining we see for CEACAM1 positive epithelial cells grown on plastic. When the fusion protein is transfected into HeLa cells and grown on laminin-coated slides, the cells attach poorly due to the lack of surface expression of α3 integrin, but do form some cell-cell adhesion groups in which the CEACAM1–4S and F-actin co-localize between the cells (Fig. 5*C*). When the same cells are grown on plastic they attain a flattened morphology exhibiting distinct regions of co-localization between CEACAM1–4S and F-actin (Fig. 5*D*). Whereas the reason for this complex expression pattern is not apparent, we show the results to demonstrate that co-localization of the two molecules is not due to the trivial reason that both are expressed at the plasma membrane. When CEACAM1–4S-eGFP is expressed in Jurkat cells that are plated onto fibronectin-coated slides, the fusion protein is localized to the cell surface in distinct microdomains (Fig. 5, *E* and *F*). When the cells contact each other, they form cell-cell interactions in which all of the fusion protein migrates to the cell-cell boundary (Fig. 5*G*). Although these boundaries demonstrate co-localization with F-actin, we cannot conclude that the co-localization is significant because the F-actin has a cortical distribution in these cells. However, when these cells are treated with either nocodozole, a potent microtubule-disrupting reagent, or cytochalasin B, an actin polymerization disrupting agent, the cells expel a membrane bleb at the substrata attachment point that is enriched in both F-actin and CEACAM1–4S (data only shown for nocodazole, see below). In both cases, the bleb shows substantial co-localization of both molecules. Clearly, these phenomena involve a substantial rearrangement of the cytoskeleton. Because these treatments allow visual quantification of the degree of co-localization of the two molecules, we used this assay to determine whether the F454A mutation in the cytoplasmic domain of CEACAM1–4S that affected actin binding in the yeast two-hybrid assay was functional. As shown in Fig. 5, *H–M*, the wild-type fusion protein exhibits high correlation of co-localization of the two molecules (about 80%), whereas the F454A mutant shows reduced ability to co-localize the two (about 30%). The reduced ability of the mutant to co-localize with F-actin demonstrates that the mutant has a profound, but not total effect, upon F-actin localization during a process that involves substantial cytoskeletal rearrangement.

A second assay that involves substantial cytoskeletal rearrangements is the three-dimensional model of mammary morphogenesis in which MCF7 cells transfected with CEACAM1–4S form acini with lumena when grown in Matrigel for 6 days. When vector control transfected MCF7 cells are grown in a sandwich Matrigel assay (see "Materials and Methods") they form acini without lumena as seen by phase-contrast microscopy and by staining with phalloidin (actin) and 4′,6-diamidino-2-phenylindole (nuclei) in Fig. 6, *A–C*. When the Matrigel is paraffin-embedded and analyzed by immunohistochemistry, only background staining for CEACAM1 is

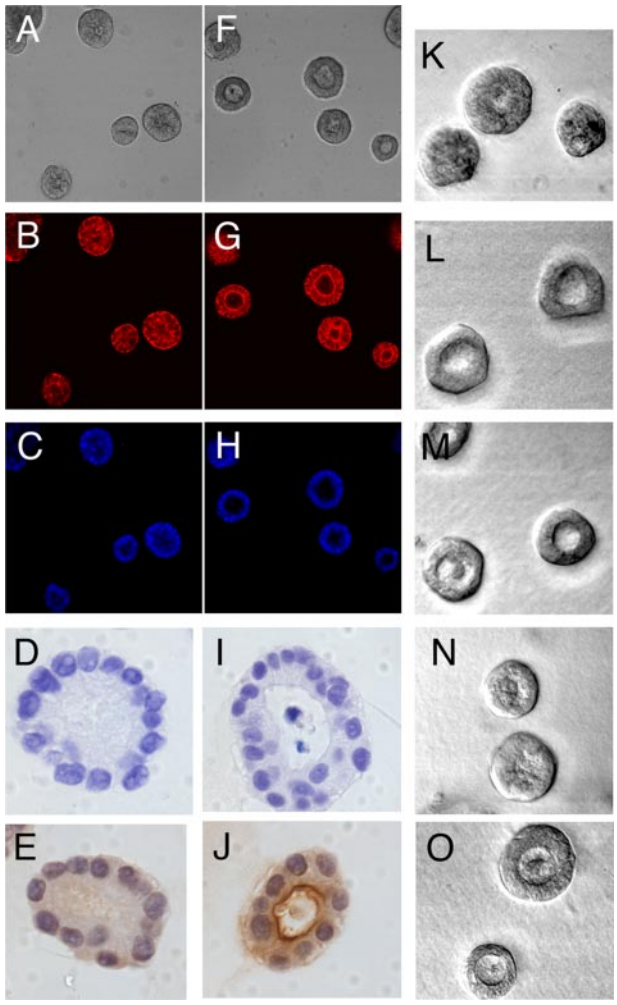

FIGURE 6. **Effect of mutational analysis on CEACAM1–4S in transfected MCF7 cells grown in Matrigel.** *A–E*, MCF7 wild-type cells were grown in sandwich Matrigel for 6 days and examined by phase-contrast microscopy (*A*) or confocal microscopy after staining with Texas Red-phalloidin (*B*) or 4′,6-diamidino-2-phenylindole (*C*). Matrigel was paraffin embedded and analyzed by H&E (*D*) or stained for CEACAM1 with monoclonal antibody 4D1C2 (*E*). Similarly, MCF7 cells transfected with wild-type CEACAM1–4S were analyzed by the same methods (*F–J*). Phase-contrast microscopy of the mutant forms of CEACAM1–4S are shown in *K–O*: F454A (*K*), T457A (*L*), S459A (*M*), double mutant T457A,S459A (*N*), and double mutant T457D,S459D (*O*).

observed (Fig. 6, *D–E*). When MCF7 cells transfected with wild-type CEACAM1–4S are grown in the sandwich Matrigel assay, lumena with a defined ring of actin are observed and the staining for CEACAM1 is localized to the luminal surface (Fig. 6, *F–J*). When MCF7 cells containing the F454A mutant were analyzed, the percent lumen formation was reduced to that found for vector control (Table 1, Fig. 6*K*). Overall, the F454A mutant-transfected cells form 6-fold less acini with lumena compared with wild-type-transfected cells. Because CEACAM1 and actin both exhibit intense staining at the luminal surface, and the F454A mutation disrupts this interaction, we conclude that Phe^{454} is the critical actin binding residue in CEACAM1–4S. We further conclude that the direct interaction of CEACAM1–4S with actin is physiologically important, and that CEACAM1–4S is a major effector in the cytoskeletal rearrangements required for lumen formation in this model.

Thr^{457} Plays a Critical Role in Apoptosis—Further examination of the sequence of the cytoplasmic domain of

TABLE 1

Lumen formation of the CEACAM1–4S mutants in Matrigel

MCF7 cells (1×10^5 per well) transfected with vector control, wild-type, or mutated CEACAM1–4S were grown in a sandwich Matrigel assay for 6 days, and 300 acini with diameters less than 50 μm were scored for well defined lumen formation. The two sets of numbers are the results of two independent experiments. *p* values were calculated by Fisher's Exact test, comparing total lumen of CEACAM1–4S wild-type and mutants to the vector-transfected MCF7 cells.

Cells	Lumen		*p* values	
	%			
Vector	14	10		
Wild-type	97	93	<0.0001	<0.0001
T457D	95	92	<0.0001	<0.0001
S459D	90	83	<0.0001	<0.0001
T457D,S459D	92	90	<0.0001	<0.0001
T457A	90	86	<0.0001	<0.0001
S459A	91	89	<0.0001	<0.0001
T457A,S459A	18	12	0.22	0.51
F454A	16	11	0.57	0.79

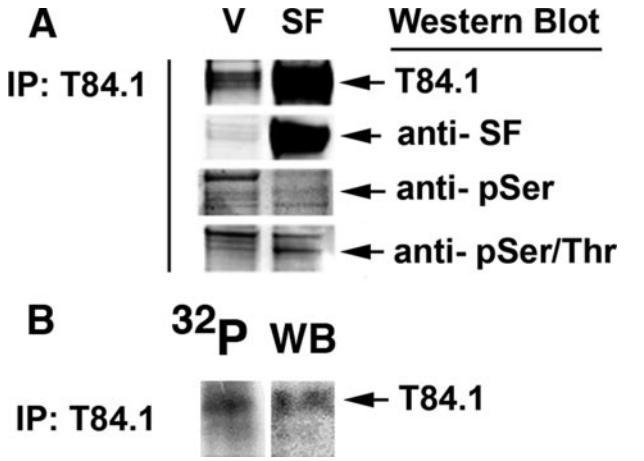

FIGURE 7. **Phosphorylation of CEACAM1–4S in transfected MCF7 cells grown in Matrigel.** *A*, MCF7 cells were transfected with empty vector (*V*) or CEACAM1–4S (*SF*), grown in Matrigel for 3 days, harvested with Matrisperse, and cell lysates immunopreciptated with anti-CEACAM1 antibody T84.1, proteins separated by SDS-gel electrophoresis, and Western blotted with T84.1, CEACAM1 short-form specific antibody 22-9 (anti-SF), and either anti-phospho-Ser or a combination of anti-phospho-Ser/Thr antibodies. *B*, MCF/CEACAM1–4S cells were grown in Matrigel with phosphate-free medium including $^{32}P_i$ for 3 days, the cells were harvested with Matrisperse, and cell lysates were immunoprecipitated with anti-CEACAM1 antibody T84.1 and proteins separated by SDS-gel electrophoresis. *Left*, autorad. *Right*, Western blot with anti-CEACAM1 antibody T84.1.

CEACAM1–4S reveals the presence of Thr^{457} and Ser^{459}, residues that have been previously shown to be phosphorylated in murine CEACAM1 and predicted to be phosphorylated in human CEACAM1 (35). To demonstrate that these residues are phosphorylated in human CEACAM1, CEACAM1–4S-transfected MCF7 cells were grown in three-dimensional culture with or without $^{32}P_i$, cells were harvested and lysed, CEACAM1 was immunoprecipitated and proteins run on SDS gels, and the gels probed for ^{32}P by autoradiography or Western blotting with anti-phospho-Ser/Thr antibodies. The results shown in Fig. 7 demonstrate that CEACAM1 is indeed phosphorylated under these conditions and that there is evidence for phospho-Thr on the Western blots. To confirm these data, mutational analysis of Thr^{457} and Ser^{459} was performed (Thr/Ser → Ala for neutral mutation analysis, and Thr/Ser → Asp to mimic phosphorylation). Each mutant was cloned and selected for equivalent surface expression on MCF7 cells (data not shown). In vector-transfected controls there was a minimal background level of lumen formation (10–14%) compared with 93–97% for cells transfected with wild-type CEACAM1–4S (Table 1, Fig. 6). When Thr^{457} or Ser^{459} were mutated to either Ala or Asp, no change in lumen formation was observed compared with wild-type cells; however, when both Thr^{457} and Ser^{459} were mutated to Ala, lumen formation was reduced to the level of vector control cells. In contrast, when both of these residues were mutated to Asp, mimicking phosphorylation, lumen formation was restored, comparable with wild-type-transfected cells. These results strongly suggest that phosphorylation of either Thr^{457} or Ser^{459} is critical for controlling lumen formation. Because the phospho-Thr Western blot is stronger than the phospho-Ser blot (Fig. 7*A*), we favor the explanation that phosphorylation of Ser^{459} is recruited when Thr^{457} is mutated to Ala.

Conclusion—When the extracellular domains of CEACAM1-4S interact with each other across cell-cell junctions in a three-dimensional model of mammary morphogenesis, they transmit signals that result in actin cytoskeleton reorganization and effect lumen formation via apoptosis of central cells within the acini. This is remarkable in that the short isoform of CEACAM1 has a cytoplasmic domain of only 12–14 amino acids. In most cases where cell surface receptors possess short cytoplasmic domains, they rely on membrane- or cytoplasmic-associated proteins for signal transduction. But in the case of CEACAM1–4S, this short stretch of amino acids can directly interact with actin (and other actin interacting molecules such as tropomyosin and AIIt), triggering subsequent cytoskeletal reorganization. The identification of a critical residue (Phe^{454}) in the cytoplasmic domain of CEACAM1 that is required for the actin interaction is reasonable in that the docking of hydrophobic residues into protein clefts is a major theme in protein-protein interactions. However, if the interaction occurs constitutively, then one could ask does actin always occupy these sites? The finding that the amide of Phe^{454} is deprotonated at pH 7 (most likely in the enol form) may provide an answer to this question, suggesting that protonation of the Phe^{454} amide facilitates productive binding. Charge changes at the cytoplasmic surface of the plasma membrane have been reported and involve distinct microdomains in the lipid membrane (36–38). Regarding the mechanism of the protonation, we hypothesize that Lys^{456} of CEACAM1 is involved because its modification (K456A) actually increases actin binding as shown in the yeast two-hybrid assay. Thus, in the correct context, Lys^{456} may decrease actin binding at pH 7, whereas at lower pH increased binding may occur. In addition, Ca^{2+} ion may affect binding because it can complex to adjacent membrane phospholipids changing the local pH. Because intracellular Ca^{2+} ion is normally around 10 nM in the cytoplasm and only transiently raises from micromolar to millimolar concentrations during certain cell signaling processes, Ca^{2+} ion fluxes within the cell could regulate actin binding to the cytoplasmic domain of CEACAM1–4S at the plasma membrane.

The critical role of Phe^{454} in actin binding also affects lumen formation in a three-dimensional model of mammary morphogenesis as shown by transfecting MCF7 cells with a F454A CEACAM1–4S mutant. There is also evidence that Thr^{457} and Ser^{459} play roles in lumen formation. Specifically, the double

mutation T457A,S459A blocks lumen formation in the three-dimensional model of mammary morphogenesis. Because the phosphorylation mimicking mutants T457D and/or S459D restore lumen formation, it is likely that one of these residues must be phosphorylated to enable lumen formation. At this point we have not been able to identify all of the components of the downstream signaling pathway that execute the phosphorylation steps. However, we have shown that the mechanism may be mediated by the protease calpain and involves Bax in a mitochondrial mediated process (16). Whereas much remains to be done to fill in the details of this complex process, we can state from the mutational analysis performed here, that even a short cytoplasmic domain can orchestrate sophisticated signaling events that were previously thought to require much larger protein domains.

REFERENCES

1. Obrink, B. (1997) *Curr. Opin. Cell Biol.* **9,** 616–626
2. Blau, D. M., Turbide, C., Tremblay, M., Olson, M., Letourneau, S., Michaliszyn, E., Jothy, S., Holmes, K. V., and Beauchemin, N. (2001) *J. Virol.* **75,** 8173–8186
3. Gray-Owen, S. D., Dehio, C., Haude, A., Grunert, F., and Meyer, T. F. (1997) *EMBO J.* **16,** 3435–3445
4. Virji, M., Evans, D., Griffith, J., Hill, D., Serino, L., Hadfield, A., and Watt, S. M. (2000) *Mol. Microbiol.* **36,** 784–795
5. Boulton, I. C., and Gray-Owen, S. D. (2002) *Nat. Immunol.* **3,** 229–236
6. Najjar, S. M. (2002) *Trends Endocrinol. Metab.* **13,** 240–245
7. Ergun, S., Kilik, N., Ziegeler, G., Hansen, A., Nollau, P., Gotze, J., Wurmbach, J. H., Horst, A., Weil, J., Fernando, M., and Wagener, C. (2000) *Mol. Cell* **5,** 311–320
8. Markel, G., Wolf, D., Hanna, J., Gazit, R., Goldman-Wohl, D., Lavy, Y., Yagel, S., and Mandelboim, O. (2002) *J. Clin. Investig.* **110,** 943–953
9. Kammerer, R., Stober, D., Singer, B. B., Obrink, B., and Reimann, J. (2001) *J. Immunol.* **166,** 6537–6544
10. Iijima, H., Neurath, M. F., Nagaishi, T., Glickman, J. N., Nieuwenhuis, E. E., Nakajima, A., Chen, D., Fuss, I. J., Utku, N., Lewicki, D. N., Becker, C., Gallagher, T. M., Holmes, K. V., and Blumberg, R. S. (2004) *J. Exp. Med.* **199,** 471–482
11. Chen, C. J., and Shively, J. E. (2004) *J. Immunol.* **172,** 3544–3552
12. Neumaier, M., Paululat, S., Chan, A., Matthaes, P., and Wagener, C. (1993) *Proc. Natl. Acad. Sci. U. S. A.* **90,** 10744–10748
13. Nittka, S., Gunther, J., Ebisch, C., Erbersdobler, A., and Neumaier, M. (2004) *Oncogene* **23,** 9306–9313
14. Huang, J., Simpson, J. F., Glackin, C., Riethorf, L., Wagener, C., and Shively, J. E. (1998) *Anticancer Res.* **18,** 3203–3212
15. Huang, J., Hardy, J. D., Sun, Y., and Shively, J. E. (1999) *J. Cell Sci.* **112,** 4193–4205
16. Kirshner, J., Chen, C. J., Liu, P., Huang, J., and Shively, J. E. (2003) *Proc. Natl. Acad. Sci. U. S. A.* **100,** 521–526
17. Nollau, P., Scheller, H., Kona-Horstmann, M., Rohde, S., Hagenmuller, F., Wagener, C., and Neumaier, M. (1997) *Cancer Res.* **57,** 2354–2357
18. Luo, W., Tapolsky, M., Earley, K., Wood, C. G., Wilson, D. R., Logothetis, C. J., and Lin, S. H. (1999) *Cancer Gene Ther.* **6,** 313–321
19. Luo, W., Wood, C. G., Earley, K., Hung, M. C., and Lin, S. H. (1997) *Oncogene* **14,** 1697–1704
20. Kleinerman, D. I., Dinney, C. P., Zhang, W. W., Lin, S. H., Van, N. T., and Hsieh, J. T. (1996) *Cancer Res.* **56,** 3431–3435
21. Schumann, D., Chen, C.-J., Kaplan, B., and Shively, J. E. (2001) *J. Biol. Chem.* **276,** 47421–47433
22. Edlund, M., Blikstad, I., and Obrink, B. (1996) *J. Biol. Chem.* **271,** 1393–1399
23. Kirshner, J., Schumann, D., and Shively, J. E. (2003) *J. Biol. Chem.* **278,** 50338–50345
24. Gunning, P., Leavitt, J., Muscat, G., Ng, S. Y., and Kedes, L. (1987) *Proc. Natl. Acad. Sci. U. S. A.* **84,** 4831–4835
25. Mayer, M., and Meyer, B. (2001) *J. Am. Chem. Soc.* **123,** 6108–6117
26. Yu, E. W., McDermott, G., Zgurskaya, H. I., Nikaido, H., and Koshland, D. E., Jr. (2003) *Science* **300,** 976–980
27. Otterbein, L. R., Cosio, C., Graceffa, P., and Dominguez, R. (2002) *Proc. Natl. Acad. Sci. U. S. A.* **99,** 8003–8008
28. Holmes, K. C., Schroder, R. R., Sweeney, H. L., and Houdusse, A. (2004) *Philos. Trans. R. Soc. Lond. B Biol. Sci.* **359,** 1819–1828
29. Dauber-Osguthorpe, P., Roberts, V. A., Osguthorpe, D. J., Wolff, J., Genest, M., and Hagler, A. T. (1988) *Proteins* **4,** 31–47
30. Dominguez, R. (2004) *Trends Biochem. Sci.* **29,** 572–578
31. Lorenz, M., Poole, K. J., Popp, D., Rosenbaum, G., and Holmes, K. C. (1995) *J. Mol. Biol.* **246,** 108–119
32. Holmes, K. C., Angert, I., Kull, F. J., Jahn, W., and Schroder, R. R. (2003) *Nature* **425,** 423–427
33. Watt, S. M., Teixeira, A. M., Zhou, G. Q., Doyonnas, R., Zhang, Y., Grunert, F., Blumberg, R. S., Kuroki, M., Skubitz, K. M., and Bates, P. A. (2001) *Blood* **98,** 1469–1479
34. Kirshner, J., Hardy, J., Wilczynski, S., and Shively, J. E. (2004) *J. Mol. Histol.* **35,** 287–299
35. Edlund, M., Wikstrom, K., Toomik, R., Ek, P., and Obrink, B. (1998) *FEBS Lett.* **425,** 166–170
36. Kano, K., and Fendler, J. H. (1978) *Biochim. Biophys. Acta* **509,** 289–299
37. Wallach, D. F. (1976) *J. Cell Physiol.* **89,** 769–770
38. Yeung, T., Terebiznik, M., Yu, L., Silvius, J., Abidi, W. M., Philips, M., Levine, T., Kapus, A., and Grinstein, S. (2006) *Science* **313,** 347–351
39. Spaar, A., and Salditt, T. (2003) *Biophys. J.* **85,** 1576–1584
40. Heller, H., Schaefer, M., and Schulten, K. (1993) *J. Phys. Chem.* **97,** 8343–8360